Regular Article

Check for updates

Cross-diffusion of magnetohydrodynamic Williamson and Casson fluid flow past a slendering horizontal surface with variable thickness and multi-slip conditions: an implicit finite difference approach

Ram Prakash Sharma[1,a] **, Thirupathi Thumma**[2]**, S. R. Mishra**[3]**, Sunendra Shukla**[4]

[1] Department of Mechanical Engineering, National Institute of Technology Arunachal Pradesh, Papum Pare 791113, India
[2] Department of Mathematics, B V Raju Institute of Technology, Narsapur, Medak, Telangana State 502313, India
[3] Department of Mathematics, Siksha 'O' Anusandhan Deemed to be University, Khandagiri, Bhubaneswar, Odisha 751030, India
[4] Department of Basic and Applied Science, National Institute of Technology Arunachal Pradesh, Papum Pare 791113, India

Abstract The influence of cross-diffusion effects for the roles of Soret and Dufour effects within the context of the flow of two-dimensional Williamson and Casson fluids over an elongated sheet with varying thicknesses is analyzed. The properties of the magnetic field along with multi-slip boundary conditions are also explored in this investigation. In engineering, the assumption of a fully developed flow is often used to design a mathematical model with the governing equations of the flow profile in the form of partial differential equations. With the aid of an implicit finite difference approach, the set of nonlinear coupled transformed problems is solved followed by similarity transformation that is useful for the conversion of non-dimensional form. The impact of these processes on the fluid flow phenomena parameterized by different non-dimensional parameters has been discussed. Moreover, the rate constants such that the skin friction coefficient and heat transfer rate characteristics are widely scrutinized with the support of various plots and tables.

List of symbols

C	Concentration of fluid
C_f	Skin friction coefficient
C_p	Specific heat capacity
C_s	Concentration susceptibility
C_∞	Concentration at free stream
D_m	Molecular diffusivity
Du	Dufour number
f	Dimensionless velocity
h_1	Dimensionless velocity slip
h_2	Dimensionless temperature jump
h_3	Dimensionless concentration jump
h_1^*	Dimensional velocity slip parameter
h_2^*	Dimensional temperature jump parameter
h_3^*	Dimensional concentration jump parameter
k	Thermal conductivity (w/mk)
k_T	Thermal diffusion ratio
m	Velocity power index parameter
Pr	Prandtl number
M	Magnetic interaction parameter
Nu_x	Local Nusselt number
Re_x	Local Reynolds number
Sc	Schmidt number
Sr	Soret number
Sh_x	Local Sherwood number

[a] e-mail: rpsharma@nitap.ac.in (corresponding author)

T Temperature of the fluid (K)
T_∞ Temperature of the fluid in the free stream (K)
u, v Velocity components in x and y directions (m/s)

Greek symbols

ϕ Dimensionless concentration
η Similarity variable
σ Fluid electrical conductivity
θ Dimensionless temperature
ρ Density of the fluid $\left(\text{kg/m}^3\right)$
Λ Williamson fluid parameter
μ Dynamic viscosity
υ Kinematic viscosity $\left(\text{m}^2/\text{s}\right)$
λ Wall thickness parameter
ξ Mean free path (constant)
Γ Positive characteristic time
β Casson parameter

1 Introduction

Double diffusion effects refer to the simultaneous influence of two different diffusion processes, often involving temperature and concentration gradients, on the behavior of fluids. This phenomenon plays a pivotal role in various natural and industrial processes, such as ocean currents, crystal growth, and biological systems. When temperature and concentration gradients coexist, intricate interactions occur, leading to unique phenomena like thermohaline convection and solutal buoyancy-driven flows. Understanding double diffusion is crucial for comprehending complex transport mechanisms and their impact on diverse physical systems. Double diffusion occurs in fields including oceanography, astrophysics, and chemical engineering, offering insights into diverse thermodynamic applications like enhanced refrigeration, cooling for electronic devices, and optimized heat exchangers. Beghein et al. [1] have explored its potential to enhance efficiency in chemical processes and engineering applications. Qiang et al. [2] examined the diffusion thermal effect of unsteady magnetohydrodynamic (MHD) convective flow between two infinitely vertical parallel plates. This investigation considered the presence of both a magnetic field and a synthetic reaction, utilizing integral transformation techniques. The researchers conducted a thorough analysis, comparing graphical representations of analytical and semi-analytical outcomes. Sreedevi et al. [3] elucidated the numerical solution of the combined effect of radiation, varying viscosity, and effect of Hall current toward the stretching sheet of an MHD free-convective flow for the inclusion of heat generation/absorption. They have employed used the fifth-order R-K Fehlberg procedure along with the shooting performance and discussed the numerous physical factors affecting the flow phenomena. Sathiyamoorthi and Anbalagan [4] investigated the phenomenon of dual-diffusive free transmission within an inclined crater. They examined the impact of magnetic effects on this process by employing Bejan's concepts of heat and mass transport phenomena. Their analysis was conducted utilizing the lattice Boltzmann method (LBM). Kefayati et al. [5] analyzed the double-diffusion free convection flow of non-Newtonian power-law liquids in various cavities, showing the flat magnetic effect, and corrected Soret and Dufour factors by using FDLBM. The simulation of heat and mass transfer parameters such as power-law exponent, Lewis number, Soret and Dufour parameter, and other parameters are discussed in detail. Mondal and Mohapatra [6] proposed the problem of double-diffusion mixed transmission of nanofluids in trapezoidal shells with various aspect ratios in the presence of a magnetic field and the results are deployed numerically. They analyzed the production of entropy to develop the competence of numerous thermodynamic tools, such as refrigeration, microchip technology, cooling and heat exchangers, and more.

Many studies of laminar flow and heat transportation past an expanding sheet, such as glass fiber and metal and polymer extrusion, involve heating procedures at extraordinary temperatures due to the thermal radiation effect. The end product of such manufacturing procedures is subject to the rate of cooling during production. Devi and Prakash [7] analyzed the laminar flow and heat transmission of variable thickness expanding sheets with thermal radiation in the existence of a magnetic field. They have used the Runge–Kutta fourth-order integration method equipped with a shooting technique for the solution of the proposed designed model. They found that developing the magnetic effect suppresses the heat transfer rate and the thermal emission enhances additional heat so need to maintain the physical conditions. Devi and Prakash [8] investigated numerically the steady, incompressible hydromagnetic flow toward a slender sheet with a varying magnetic field and thermal conductivity. They found that temperature-dependent viscosity declines the fluid temperature but developing the thermal conductance enhances the thermal rate of the fluid. Reddy et al. [9] elucidated the hydromagnetic unsteady motion of a nanoliquid past a slender expanding sheet with slip effects and thermophoresis and Brownian motion. They procured deploying the R-K-Fehlberg method and found that thermophoresis and Brownian parameters can enhance

the fluid temperature significantly. Elattar et al. [10] addressed the computing approach for the steady flow of a hybrid nanoliquid in the existence of Hall current along with the impact of variable magnetic field and chemical reactions over an impermeable slandering sheet. Prasad et al. [11] investigated the characteristics of magnetohydrodynamic (MHD) heat transport in a nanoliquid flowing over a delicate, elastic surface. They examined the influence of different layer spacings and variations in the physical properties of the liquid. Employing the optimal homotopy asymptotic method (OHAM), they derived results concerning the nanofluid's motion and heat transfer behavior. The concept of variable thickness surface is created from linearly deformable substances such as needles and nozzles. Variable thickness sheets are more often encountered in practical applications. Variable-thickness stretched sheets may appear more frequently in engineering applications than flat sheets. Adaptable thickness panels are common usage in appliance models, construction, atomic apparatus machinery, marine structural and acoustic component panels, machine design, and buildings and construction. For sheets with variable stretch speeds at altered points, the thickness of the expanse can vary as the sheet moves. Historically, the first study of boundary layer motion through an elongated sheet with inconstant thickness was recognized in motion through a variable diameter needle discussed by Lee [12]. Zhang et al. [13] revisited the flow of boundary layers on continuously stretched sheets with power-law surface velocities and variable thicknesses. They mainly discussed the parameters' velocity power index on the behavior of boundary layer flow. The generalized heat flux phenomena for nonlinear convection of dissipative Casson MHD fluid across a narrow stretching sheet is examined by Akolade et al. [14] when multi-slip and Soret–Dufour effects are profound. Elayarani et al. [15] statistically investigated the gyrotactic microbe flow of the Carreau nanofluid stream on a horizontal slendering surface in the presence of multiple slips and radiative heat flux using the ANFIS (Adaptive neuro-fuzzy inference system). They used the implicit FDM and further discussed the various parameters affecting the flow phenomena. Hayat et al. [16] explored the MHD immobility region for the flow of Jeffery fluid past an elongating sheet through irregular thickness and they found the combined characteristics of melting effect, internal heat generation, and viscous distraction. Yusuf et al. [17] scrutinized the stimulation of the heat and mass transportation mechanism of Casson–Williamson nanofluids on stretched sheets embedded in porous media by viscous dissipation, uniform magnetic field, and velocity slip BCs. Wakif et al. [18] quantitatively examine the impacts of temperature-dependent dynamic viscosity and thermal conductivity on Casson fluid flow over moving slendering surfaces by applying a generalized differential quadrature technique. Akolade and Tijani [19] studied constant transport features on the magnetized 3-D flow of Casson–Williamson liquids through non-aligned radiation stimulus toward a Riga plate utilizing the nanoliquid by using the SQL method for stability and uniqueness. They found this in their comparative study for both liquids. Ogunseye et al. [20] investigated the mathematical solution of Casson–Williamson responsive nanoliquid species in a moving perpendicular media using a spectral quasi-linearization technique and discussed the thermodynamic properties of the fluid. They have also applied activation energy and variable heat sources/sinks in biotechnology, chemical engineering, thermal science, food processing, and more.

Kumaran and Sandeep [21] deliberated the theoretical diffusion of heat and mass influence of MHD Williamson and Casson liquids past an upper paraboloid of insurgency using the Runge–Kutta-based shooting technique. They observed that Williamson liquid is fully encouraged by the Lorentz effect when equated to the Casson fluid. Seid et al. [22] studied the multiple slips, Soret, and Dufour effects that occur within a porous media when the boundary layer flows of conducting nanoliquid through an expanding sheet. The system is influenced by the inclusion of magnetic fields, thermal radiation, heat sources, and chemical reaction. Further, using a more efficient OHAM technique the system of governing equations is solved that are equipped with various contributing constraints. Their research provides practical applications in developing the working efficiency of numerous flow-related systems and industrial activities. Thumma et al. [23] have examined the dissipative magnetic fluid flow over a nonlinear inclined expanding/shrinking surface with the impact of the heat source effect. Again, Thumma et al. [24] analyzed the generalized differential quadrature rule for the three-dimensional MHD radiating dissipative Casson fluid flow having nano-sized tiny particles.

Based upon aforesaid literature and to the authors' best understanding, there is little attention on the non-Newtonian flow behavior with variable thickness surface. However, initially, Khader and Mogahed [25] reported the flow behavior under the influence slip condition. The present work is an extended work of Babu and Sandeep [26] by the inclusion of hydromagnetic thermal and species boundary layer influence by multi-slip conditions. On the other hand, Aliy and Kishan [27] investigated EMHD Williamson fluid on the surface with non-uniform thickness taking viscous dissipation. Later on, the problem is also extended by considering radiative heat flux by Sharma et al. [28], but they ignored external magnetic strength influence. Therefore, in this article, we strive to find suitable numerical solutions to the nonlinear problem in the occurrence of 2-D cross-diffusion for both Williamson and Casson fluids flowing through elongated sheets of variable thickness on magnetohydrodynamics have been discussed by observing multi-slip conditions. The method uses boundary layer theory and similarity solutions. We obtain flow profiles in terms of flow, heat, and mass including various parameters. The complete problem with chemically reactive species (mass and heat transfer) has been reduced to ODEs, which are then solved by employing the implicit finite difference technique. The effects of skin friction coefficient, local Nusselt number, and Sherwood number were also analyzed.

2 Mathematical model and analysis

The steady 2-D and laminar MHD flow of Williamson and Casson liquid over an expanding surface with non-uniform thickness is considered in the present analysis. The $\tilde{x}$-axis is considered alongside the surface of the flow, and the $\tilde{y}$-axis is taken normal to

Fig. 1 Schematic diagram of the flow model
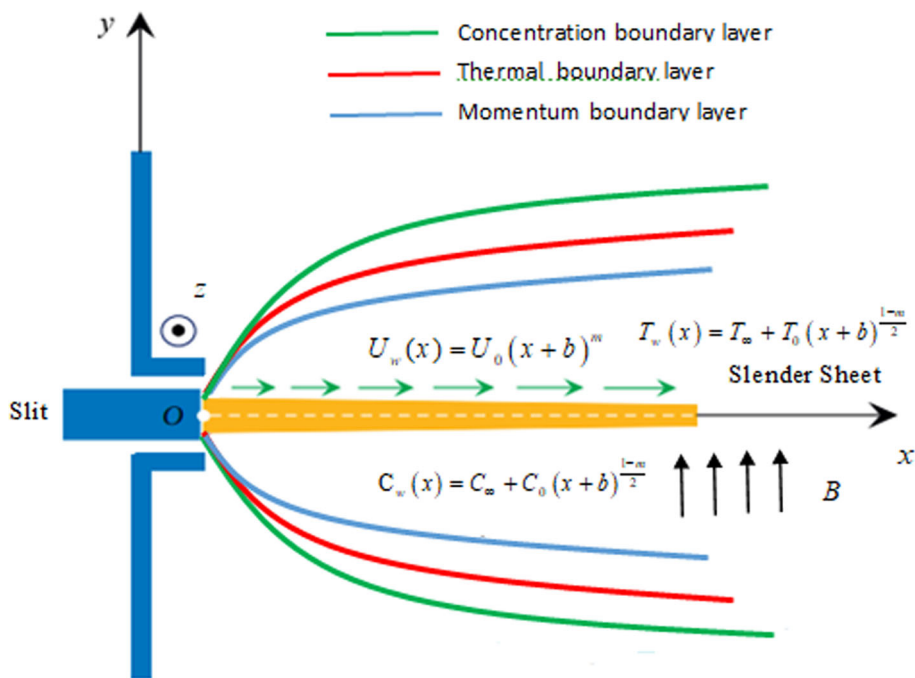
the surface. Let,$U_w(\tilde{x}) = U_0(\tilde{x} + b)^m$ is the sheet velocity, $\tilde{y} = A(\tilde{x} + b)^{1-m/2}$, $v_w = 0$ for $m \neq 1$ is assumed. Because of the low magnetic Reynolds number, the effect of induced magnetic effect is not taken into account; however, the transverse magnetic field of strength is applied along the normal direction of the flow. Here, due to the cross-diffusion, the joint impact of the Soret and Dufour effect is deliberated (Fig. 1).

The basic steady-state equations for the 2-D laminar flow of the Casson and Williamson fluids are [28]

$$\partial \tilde{u}/\partial \tilde{x} + \partial \tilde{v}/\partial \tilde{y} = 0, \tag{1}$$

$$\tilde{u}\left(\partial \tilde{u}/\partial \tilde{x}\right) + \tilde{v}\left(\partial \tilde{u}/\partial \tilde{y}\right) = \tilde{v}\left(1 + 1/\beta\right)\left(\partial^2 \tilde{u}/\partial \tilde{y}^2\right) - \sqrt{2}\tilde{v}\Gamma\left(\partial \tilde{u}/\partial \tilde{y}\right)\left(\partial^2 \tilde{u}/\partial \tilde{y}^2\right) - \left(\sigma B^2(\tilde{x})/\rho\right)\tilde{u}, \tag{2}$$

$$\tilde{u}\left(\partial T/\partial \tilde{x}\right) + \tilde{v}\left(\partial T/\partial \tilde{y}\right) = k/\rho C_p\left(\partial^2 T/\partial \tilde{y}^2\right) + \left(D_m k_T/C_s C_p\right)\left(\partial^2 C/\partial \tilde{y}^2\right), \tag{3}$$

$$\tilde{u}\left(\partial C/\partial \tilde{x}\right) + \tilde{v}\left(\partial C/\partial \tilde{y}\right) = D_m\left(\partial^2 C/\partial \tilde{y}^2\right) + \left(D_m k_T/T_m\right)\left(\partial^2 T/\partial \tilde{y}^2\right), \tag{4}$$

The corresponding usual BCs are

$$\left.\begin{array}{l}
\tilde{u}(\tilde{x}, \tilde{y}) = U_w(\tilde{x}) + h_1^*\left(\partial \tilde{u}/\partial \tilde{y}\right), \tilde{v}(\tilde{x}, \tilde{y}) = 0, \\[2mm]
T(\tilde{x}, \tilde{y}) = T_w(\tilde{x}) + h_2^*\left(\partial T/\partial \tilde{y}\right), C(\tilde{x}, \tilde{y}) = C_w(\tilde{x}) + h_3^*\left(\partial C/\partial \tilde{y}\right) \\[2mm]
\text{and} \\[2mm]
\tilde{u} = 0, T = T_\infty, C = C_\infty \text{ at } \tilde{y} = \infty
\end{array}\right\} \tag{5}$$

where

$$h_1^* = \left((2 - f_1)/f_1\right)\xi_1(\tilde{x} + b)^{1-m/2}, \xi_2 = \left(2\gamma/\gamma + 1\right)\xi_1/\text{Pr}, \tag{6}$$

$$h_2^* = \left((2 - a)/a\right)\xi_2(\tilde{x} + b)^{1-m/2}, \xi_3 = \left(2\gamma/\gamma + 1\right)\xi_2/\text{Pr}, \tag{7}$$

$$h_3^* = \left((2 - d)/d\right)\xi_3(\tilde{x} + b)^{1-m/2}, B(\tilde{x}) = B_0(\tilde{x} + b)^{m-1/2}, \tag{8}$$

$$T_w(\tilde{x}) - T_\infty = T_0(\tilde{x} + b)^{1-m/2} \text{ and } C_w(\tilde{x}) - C_\infty = C_0(\tilde{x} + b)^{1-m/2} \tag{9}$$

The similarity transformations:

$$\psi(\tilde{x}, \tilde{y}) = f(\eta)\left(2/m + 1 \tilde{v} U_0(\tilde{x} + b)^{m+1}\right)^{0.5} \tag{10}$$

$$\eta = \tilde{y}\left((m+1)\big/2\; U_0 \frac{(\tilde{x}+b)^{m-1}}{\upsilon}\right)^{0.5},$$ (11)

$$\theta(T_w(\tilde{x}) - T_\infty) = T - T_\infty \text{ and } \phi(C_w(\tilde{x}) - C_\infty) = C - C_\infty$$ (12)

If stream function ψ be defined as $\tilde{u} = \frac{\partial \psi}{\partial \tilde{y}}$ and $\tilde{v} = -\frac{\partial \psi}{\partial \tilde{x}}$ then $\tilde{u}$ and $\tilde{v}$ satisfies the equation of continuity and using.

$$\tilde{v} = -\sqrt{(m+1)\big/2\; \nu U_0(\tilde{x}+b)^{m-1}}\left[f'(\eta)\,\eta\left(m - 1\big/m+1\right) + f(\eta)\right] \text{ and } \tilde{u} = U_0(\tilde{x}+b)^m f'(\eta)$$ (13)

Using (12), (13) and (14), Eqs. (2)–(4) changed as the below ODEs:

$$\left(1 + 1\big/\beta\right)f''' + \Lambda f'' f''' + f'' f - 2m\big/1+m\, f'^2 - M\, f' = 0,$$ (14)

$$\theta'' + \Pr f\theta' - \Pr\left(1 - m\big/m+1\right)f'\theta + \Pr \text{Du}\, \phi'' = 0,$$ (15)

$$\phi'' + \text{Sc}\, f\phi' - \text{Sc}\left(1 - m\big/m+1\right)f'\phi + \text{Sc}\, \text{Sr}\, \theta'' = 0,$$ (16)

and the corresponding BCs are

$$\left.\begin{array}{l} f'(0) = \left[1 + h_1 f''(0)\right], f(0) = \lambda\left(1 - m\big/m+1\right)\left[1 + h_1 f''(0)\right], \\ \phi(0) = \left[1 + h_3 \phi'(0)\right], \theta(0) = \left[1 + h_2 \theta'(0)\right], \\ \phi(\infty) = 0, \theta(\infty) = 0, f'(\infty) = 0 \end{array}\right\}$$ (17)

where Λ, M, $\Pr$, Du, Sc, Sr are defined as

$$\left.\begin{array}{l} \Lambda = \Gamma\sqrt{(m+1)U_0^3\left\{(\tilde{x}+b)^{3m-1}\big/\tilde{v}\right\}}, M = 2\sigma B_0^2\big/\rho U_0(m+1) \\ \Pr = \mu C_P\big/k, \text{Du} = \left\{D_m k_T(C_w - C_\infty)\big/\tilde{v}C_s C_p(T_w - T_\infty)\right\}, \\ \text{Sc} = \tilde{v}\big/D_m, \text{Sr} = D_m k_T(T_w - T_\infty)\big/\tilde{v}T_m(C_w - C_\infty) \end{array}\right\}$$ (18)

The physical quantities of interest such as the skin friction, heat, and mass transfer rate coefficients are given by

$$C_f = 2\,\frac{\mu \partial \tilde{u}\big/\partial \tilde{y}}{\rho U_w^2}, \text{Nu}_x = \frac{(\tilde{x}+b)\partial T\big/\partial \tilde{y}}{T_w(\tilde{x}) - T_\infty}, \text{Sh}_{\tilde{x}} = \frac{(\tilde{x}+d)\partial C\big/\partial \tilde{y}}{C_w(\tilde{x}) - C_\infty}$$ (19)

$$\left.\begin{array}{l} C_f(\text{Re}_{\tilde{x}})^{0.5} = 2\left(m + 1\big/2\right)^{0.5}\left((1+\beta^{-1})f''(0) + \Lambda f''^2(0)\right), \text{Nu}_{\tilde{x}} = -\left(m + 1\big/2\right)^{0.5}\theta'(0)(\text{Re}_{\tilde{x}})^{0.5}, \\ \text{Sh}_x = -\left(m + 1\big/2\right)^{0.5}\phi'(0)(\text{Re}_{\tilde{x}})^{0.5} \end{array}\right\}$$ (20)

$$\text{Re}_x = U_w X\big/\nu \text{ and } X = (\tilde{x}+b)$$

3 Implicit finite difference approximation technique

The dimensionless coupled ordinary differential Eqs. (14)–(16) are highly nonlinear. Thus, the closed-form solutions are almost impossible. Thus, the subsequent governing equations concerning Eq. (17) are numerically solved by employing the implicit finite difference method (KBM—Keller box method). The fundamental prime steps elaborated in the Keller box scheme are outlined as follows.

- The set of ODEs is changed into a system of first-order equations. That is a system of IVPs;
- The system of initial value problems is approximated in terms of finite differences.
- Newton's method is adopted to linearize the resulting finite difference equations and then represented in vector notation.
- Finally, the set of linear equations is solved with the block tridiagonal elimination method (BTEM) by choosing suitable initial guesses.

In this study, a mesh of uniform size $h = 0.001$ is taken, and the convergence criteria 10^{-6} are considered to get the asymptotic solutions.

Table 1 Comparisons of present numerical results for various Sr, Du

Sr	Du		Babu and Sandeep [26]	Aliy and Kishan [27]	Sharma et al. [28]	Present results
0.1	0.3	$\frac{Nu_x}{\sqrt{Re_x}}$	0.4032	0.40334	0.403374	0.403373
0.3	0.3		0.3884	0.38864	0.388633	0.388631
0.5	0.3		0.3681	0.36806	0.368083	0.368084
0.5	0.1		0.3459	0.34584	0.345850	0.345851
0.5	0.3		0.2134	0.21353	0.213572	0.213574
0.5	0.5		0.1581	0.15832	0.158344	0.158341
0.1	0.3	$\frac{Sh_x}{\sqrt{Re_x}}$	0.3666	0.36686	0.366888	0.366887
0.3	0.3		0.2352	0.23532	0.235334	0.235332
0.5	0.3		0.1644	0.16417	0.164136	0.164138
0.5	0.1		0.4402	0.44013	0.440115	0.440114
0.5	0.3		0.3508	0.35092	0.350903	0.350906
0.5	0.5		0.5193	0.51948	0.519423	0.519426

4 Results and discussion

The importance of the property of magnetization on the conducting Casson–Williamson fluid flow phenomena is demonstrated in the present investigation. The significant behavior of viscous dissipation along with thermal radiation and the heat source/sink enriches the properties of the flow phenomena. The novelty of the present article arises due to the consideration of multiple slip boundary conditions. Numerical treatment such as the Keller box method is employed for the solution of the transformed model. The behavior of the characterizing parameters affecting the flow phenomena is established and presented graphically, and the simulated results of the rate coefficients are presented through tables. The code validation for the proposed methodology in a particular case is presented in Table 1. It describes that when $\beta \to \infty$ the results are in good agreement with the results reported in Babu and Sandeep [26] when $\beta \to \infty \& E_0 = Ec = 0$ the results are almost close to the semi-analytical results reported in Aliy and Kishan [27] and the absence of thermal radiation, the results of Sharma et al. [28] for the various values of Soret and Dufour numbers, the rate of heat and solutal transfer are approximated when $M = 0$ and the results of present outcomes show a good correlation. Further, the description of the method is elaborated in the corresponding section. Table 2 depicts the behavior of certain physical parameters on the rate coefficients refereeing to the Casson fluid. The simulated result shows that the enhanced magnetic parameter augments the shear rate whereas the impact shows its opposite behavior on the profiles of the heat and solutal rate coefficients. Further, a similar effect is rendered in all the profiles for the increasing behavior of the power-law index parameter. However, augmentation in the wall thickness parameter enhances the rate coefficients significantly. Table 3 portrays the characteristics of several parameters on the rate coefficients relating to the Williamson fluid. The numerical results show that the variation is equivalent to the variations presented in the case of Casson fluid, but in comparison, it reveals that the magnitude is higher in the case of Casson fluid.

Figures 2, 3, 4 illustrate the impact of magnetic parameters M on motion, heat, and mass profiles. The development of the values of the magnetic field parameters was detected to decline the velocity and rise the values of the heat and species profiles. The growth of the magnetic field is known to create resistance, which means it increases the viscosity of the liquid, and molecular bonds create the opposite resistance to fluid flow, known as the Lorentz force. This kind of force develops the heat near the surface. It is worth noting that small temperature changes are mixed manifestations of concentration profiles. In conclusion, in Williamson liquid, the velocity, heat, and species distributions are more affected than in Casson liquid due to the magnetic parameters.

The behavior of the power index parameter m on the velocity, heat, and concentration profile of Williamson and Casson liquids is shown in Figs. 5, 6, 7. It indicates the degree of non-Newtonian characteristics of the fluid. For different applications, the significance of the velocity power index m depends on the elongating surface and may decline or rise depending on the distance from the slot due to the speeding up or slowing down of the surface. When ($m < 1$), the non-flatness introduces an effect of mass suction, which produces the boundary layer thinner with higher wall drag; while when ($m > 1$), the non-flatness leads due to mass injection, which lessens the wall drag resulting in a larger thickness. For ($m = 1$) surface is treated as flat. It is depicted that the velocity profile in Williamson liquid and Casson liquid increases due to momentum boundary wideness becoming smaller as m upsurges along the surface. It is noticed that in Figs. 6 and 7, the temperature as well as concentration profile rises with growing values of m. The thickness of the temperature profile in Williamson liquid effectively increases as compared to Casson liquid due to m and the coefficient of local skin friction increasing in magnitude. Figure 8 represents the impact of Λ, β on the velocity profile of the Williamson parameter and Casson parameter. In both cases, increasing these parameters the velocity profile for both liquids velocity profile decreases significantly and the corresponding thickness of the momentum boundary layer declines with the development of the values of these parameters. Physically, these parameters are subject to yield stress, and this stress causes a resisting force and declines the velocity profile. Figure 9 shows the behavior of Pr, the Prandtl number on the temperature profile of Casson and Williamson fluid. For the enhanced Pr temperature profile decline with varying thickness in both cases. The Prandtl number controls

Table 2 Computations of $\sqrt{Re_x}C_f, \frac{Nu_x}{\sqrt{Re_x}}$ and $\frac{Sh_x}{\sqrt{Re_x}}$ at different values of M, Sr, Du, m and λ Whenever $h_1 = h_2 = h_3 = 0.25$ for *Casson fluid*

M	Sr	Du	m	λ	$\sqrt{Re_x}C_f$	$\frac{Nu_x}{\sqrt{Re_x}}$	$\frac{Sh_x}{\sqrt{Re_x}}$
0	0.3	0.3	0.75		− 7.170614	0.401155	0.283552
0.5					− 8.743520	0.382757	0.266371
1					− 10.124381	0.366153	0.251426
1.5					− 11.362697	0.350957	0.238419
1	0.1				− 10.124381	0.365955	0.258478
	0.3				− 10.124381	0.366153	0.251426
	0.5				− 10.124381	0.366344	0.244381
	0.7				− 10.124381	0.366527	0.237346
		0.1			− 10.124381	0.373274	0.251159
		0.3			− 10.124381	0.366153	0.251426
		0.5			− 10.124381	0.359034	0.251691
		0.7			− 10.124381	0.351918	0.251955
			0.2		− 7.984469	0.738343	0.389592
			0.4		− 8.822839	0.585212	0.334592
			0.6		− 9.588287	0.453986	0.285361
			0.8		− 10.296855	0.338521	0.240603
				0	− 9.939245	0.312629	0.232395
				1	− 10.124381	0.366153	0.251426
				2	− 10.313224	0.426016	0.271238
				3	− 10.505791	0.492047	0.291798

Table 3 Computations of $\sqrt{Re_x}C_f, \frac{Nu_x}{\sqrt{Re_x}}$ and $\frac{Sh_x}{\sqrt{Re_x}}$ at different values of M, Sr, Du, m and λ Whenever $h_1 = h_2 = h_3 = 0.25$ for *Williamson fluid*

M	Sr	Du	m	λ	$\sqrt{Re_x}C_f$	$\frac{Nu_x}{\sqrt{Re_x}}$	$\frac{Sh_x}{\sqrt{Re_x}}$
0	0.3	0.3	0.75	1	− 2.854348	0.287866	0.192581
0.5					− 3.518540	0.240345	0.167488
1					− 4.084987	0.202539	0.150585
1.5					− 4.585384	0.173501	0.138403
1	0.1				− 4.084987	0.202200	0.153725
	0.3				− 4.084987	0.202539	0.150585
	0.5				− 4.084987	0.202879	0.147424
	0.7				− 4.084987	0.203219	0.144241
		0.1			− 4.084987	0.205501	0.150424
		0.3			− 4.084987	0.202539	0.150585
		0.5			− 4.084987	0.199555	0.150748
		0.7			− 4.084987	0.196549	0.150911
			0.2		− 3.560392	0.576228	0.260517
			0.4		− 3.745276	0.419567	0.215649
			0.6		− 3.939110	0.287963	0.176748
			0.8		− 4.133334	0.176258	0.142344
				0	− 3.916907	0.164204	0.137281
				1	− 4.084987	0.202539	0.150585
				2	− 4.260887	0.251025	0.164796
				3	− 4.444646	0.309545	0.179978

the relative closeness in the momentum and thermal layers. The ratio of momentum and mass diffusion is well known as the Schmidt number, which is used to characterize fluid motion in the existence of momentum and mass diffusion processes. In Fig. 10, it is seen that with the increment in the Schmidt number (Sc), the concentration profile declined in both fluids due to lesser mass diffusion as compared to momentum diffusion.

Figures 11, 12, 13 demonstrate that an increase in the wall thickness parameters, denoted as λ, leads to a strong reduction in velocity, temperature, and species distributions of the Williamson and Casson liquid. This decrease in velocity profile occurs because of the behavior of λ, not all the dragging force of the expanding sheet can spread to the liquid, resulting in a decrease in friction
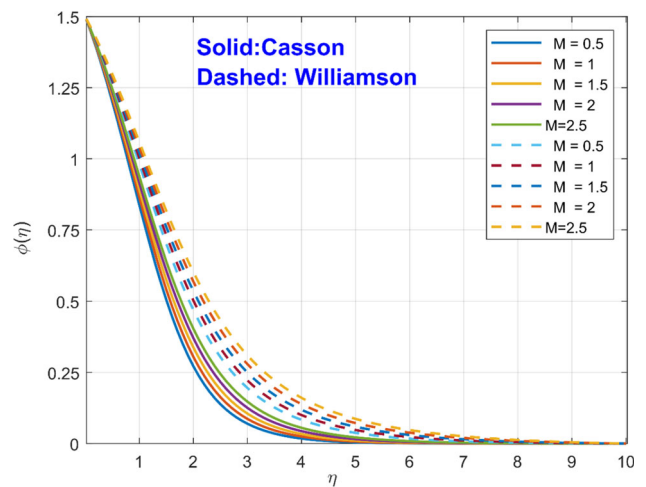
Fig. 2 Stimulus of M on velocity profiles
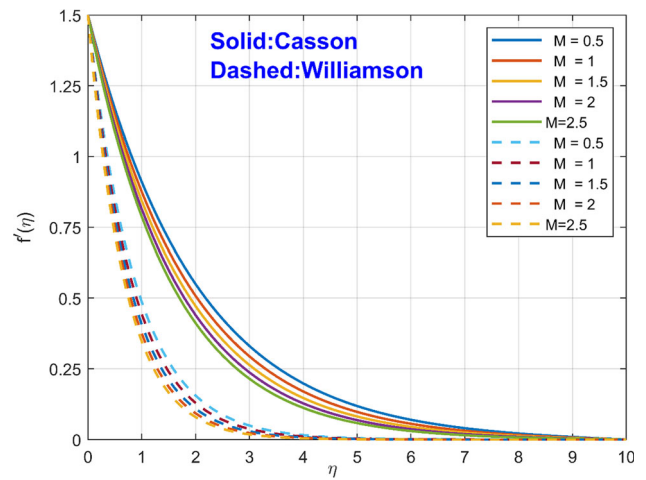
Fig. 3 Stimulus of M on energy distributions
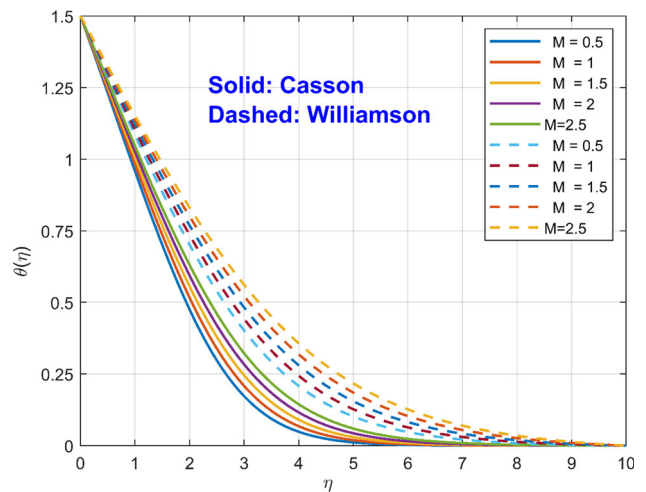
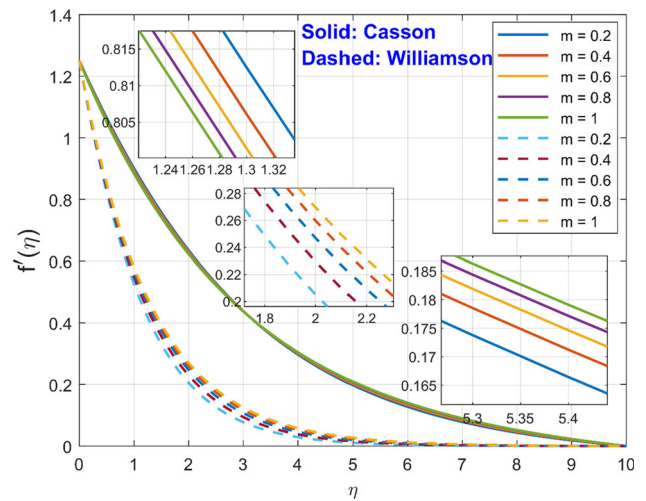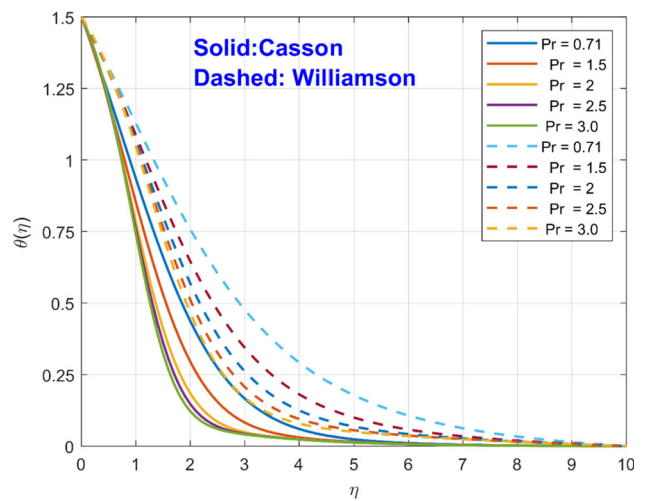**Fig. 4** Stimulus of M on concentration profiles

between fluid layers, and affecting temperature distribution. In summary, the thickness of the thermal boundary layer, as well as the concentration and temperature distribution, diminish as λ increases. Consequently, a smaller amount of heat is transferred from the surface to the liquid. Thus, both temperature distribution and concentration profile decrease due to segmentation.

Figures 14, 15, 16 reveal the collective impact of non-dimensional velocity, temperature, and concentration jump parameters h_1, h_2 and h_3 on their corresponding profile. Figure 14 shows the velocity profile increase in both the Casson and Williamson fluids, whereas from Figs. 15 and 16 it is noticed that developing the value of these parameters the temperature and concentration profile first increases up to a particular region, and afterward, the impact is reversed in both Williamson and Casson liquid. The mass flux

Fig. 5 Stimulus of m on velocity Profiles

Fig. 6 Stimulus of m on energy distributions
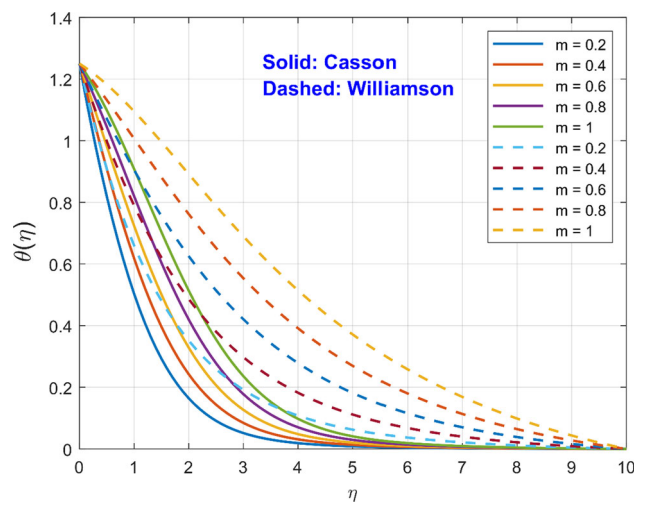
Fig. 7 Stimulus of m on concentration Profiles
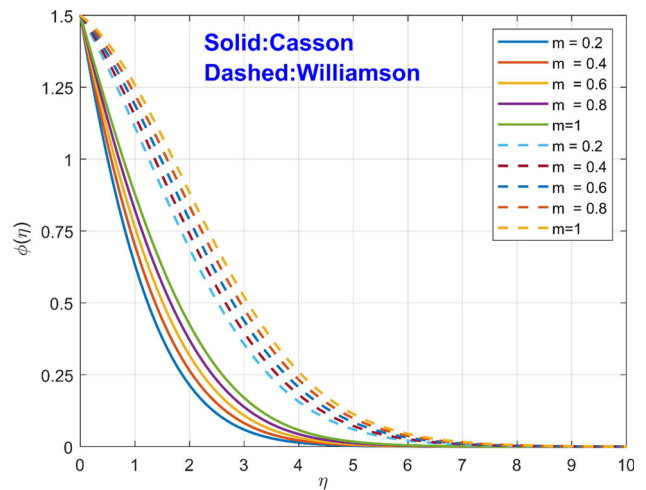
formed by a temperature gradient is known as the effect of thermal diffusion (Soret) (Sr) on concentration. Figure 17 shows the concentration distributions of Casson and Williamson liquids increase as the Soret parameter increases. In general, the characteristic of the Soret parameter increases the mass flux from the minimum concentration field to the extreme concentration field motivated by thermal gradients. Figure 18 shows the behavior of the Dufour effect on the temperature profile in both liquids. The energy flux initiated by differences in concentration/absorption is known as the diffusion-Thermo (Dufour) (Du) effect. The improving value of (Du) mixed behavior for both liquids on the temperature profile. It is physically seen that the transmission of thermal impact takes

Fig. 8 Stimulus of Λ, β on velocity Profiles
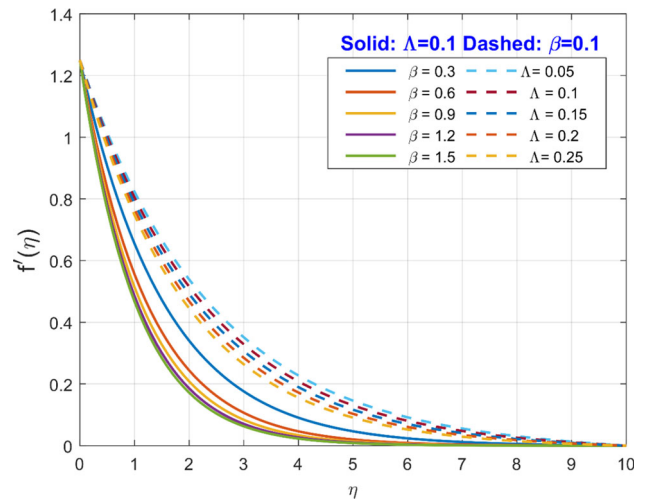
Fig. 9 Stimulus of Pr on energy distributions

Fig. 10 Stimulus of Sc on concentration Profiles
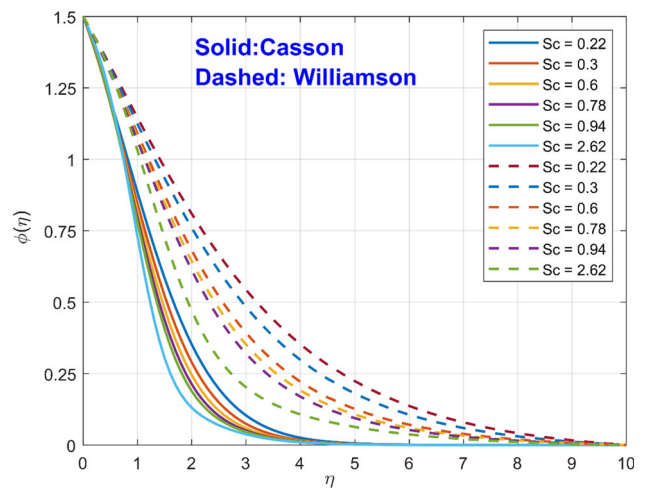

place in the energy equation and controls the thermal energy. This results in the enhancement of fluid motion and generates heat. Figure 19 encounters significant characteristics of the streamlined flow on the velocity contour concerning similarity variables in the nonexistence of magnetic parameters representing the flow pattern in the suggestive measures. Figure 20 depicts that when the magnetic parameter at a point is fixed and in the absenteeism of dimensionless parameters like h_1, h_2 and h_3 the streamlined flow on the. Similarly, in Fig. 21 velocity reflects the role in the absence of dimensionless parameters h_1, h_2 and h_3 parameter streamline flow has no change in the flow profile. Figure 22 represents the velocity profile when the $(M = 5)$ and $(m = 0.5)$ at a fixed value

Fig. 11 Stimulus of λ on velocity
Profiles
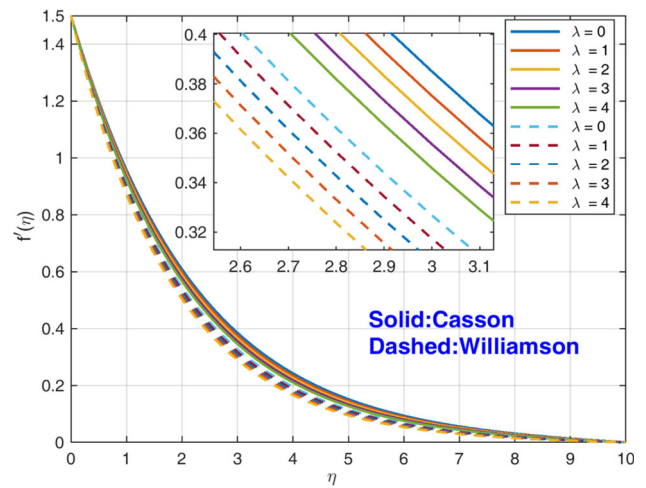
Fig. 12 Stimulus of λ on energy
distributions
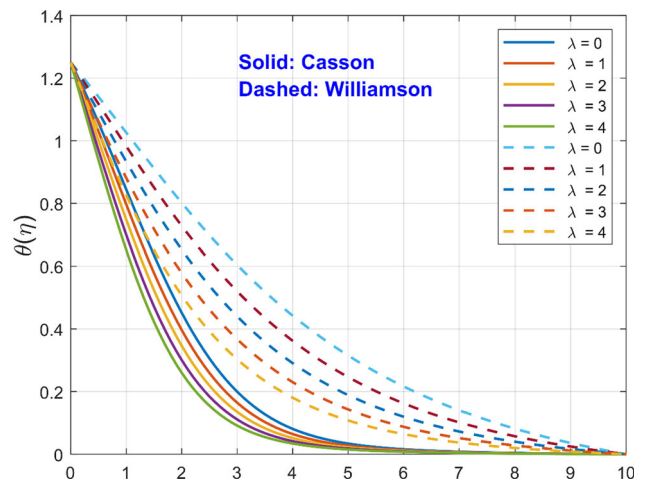
Fig. 13 Stimulus of λ on
concentration Profiles
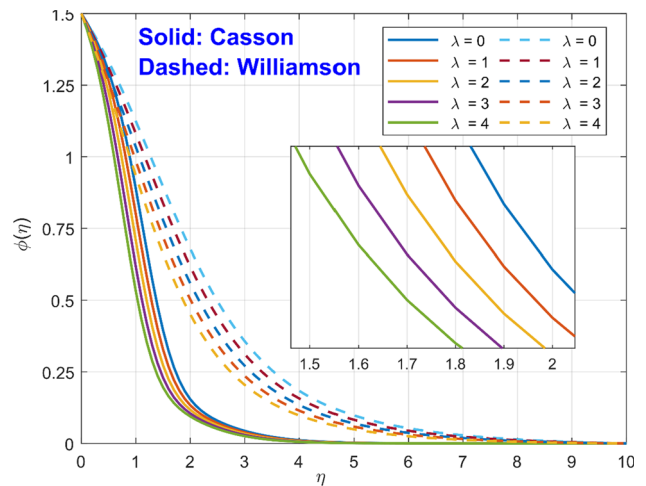
is projected as a similarity flow of the velocity boundary layer profile. Figure 23 represents the velocity boundary layer similarity flow ($m = 0.5$) and the dimensionless parameters as ($h_1 = h_2 = h_3 = 0$) there is no change in the velocity profile layer. In the absenteeism of dimensionless parameters, ($h_1 = h_2 = h_3 = 0$) streamlined flow on the velocity boundary layer looks unchanged in its similarity flow profile concerning their thickness. Figure 24 at ($M = 1$) and Fig. 25 ($m = 0.75$) display the surface plot which also shows the similarity for the distribution of velocity contour and thickness remaining unchanged.

Fig. 14 Stimulus of h_1, h_2, h_3 on velocity profiles
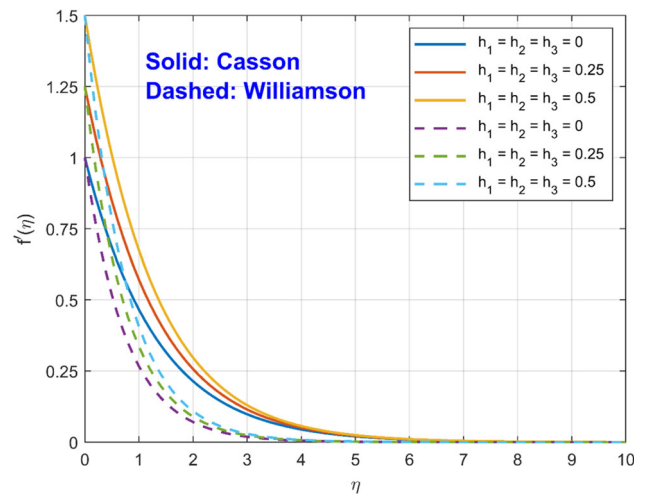
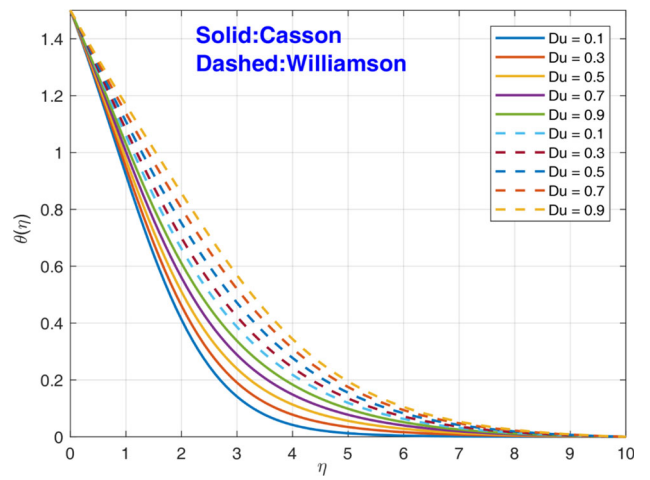**Fig. 15** Stimulus of h_1, h_2, h_3 on energy distributions
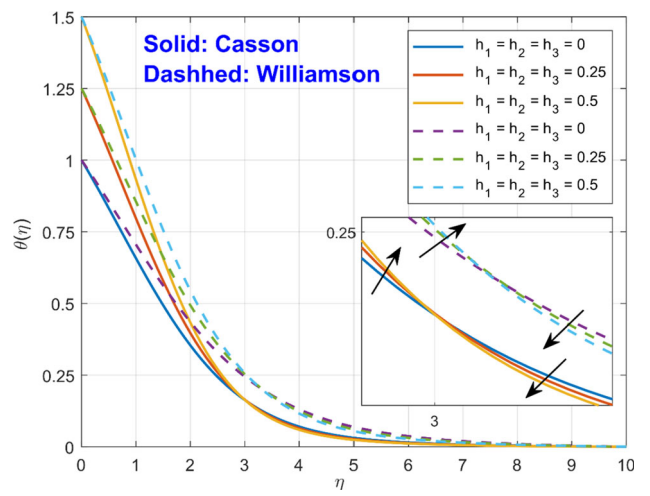
Fig. 16 Stimulus of h_1, h_2, h_3 on concentration profiles
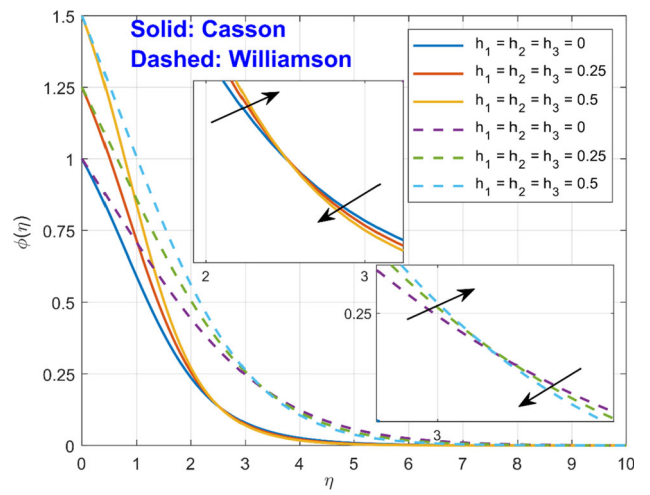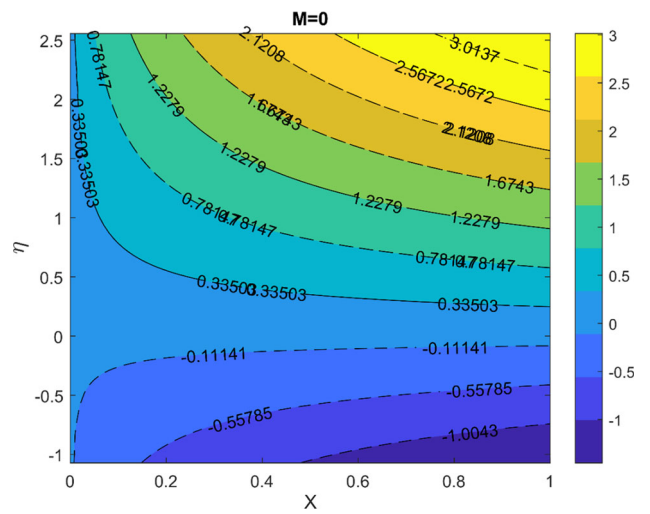
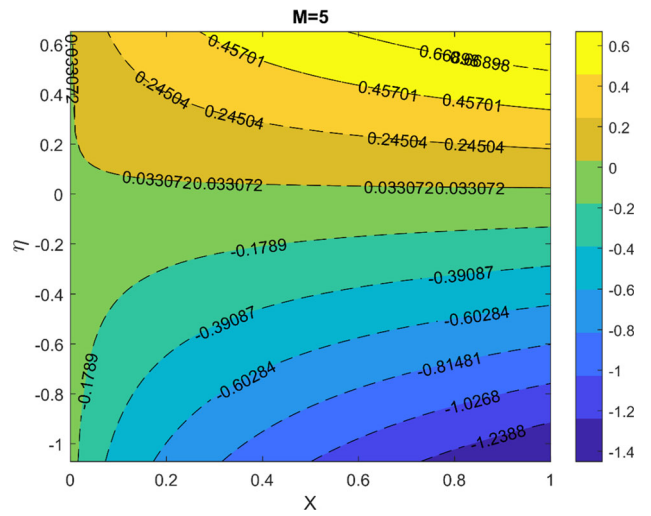**Fig. 17** Stimulus of *Sr* on concentration profiles
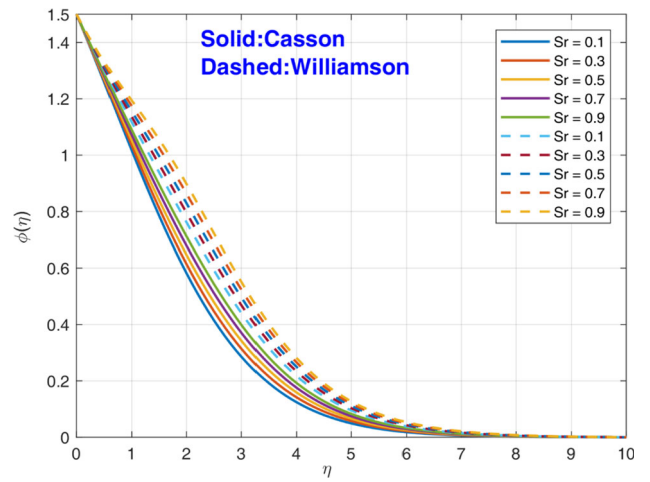
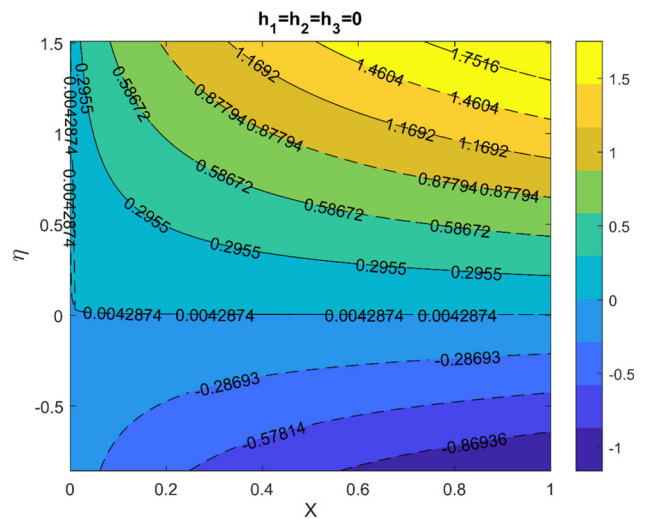
Fig. 18 Stimulus of *Du* on energy distributions
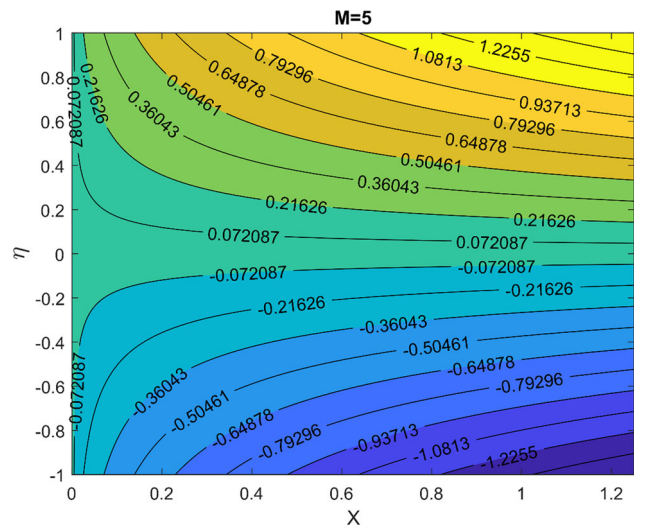

Fig. 19 Streamlines whenever $M = 0$
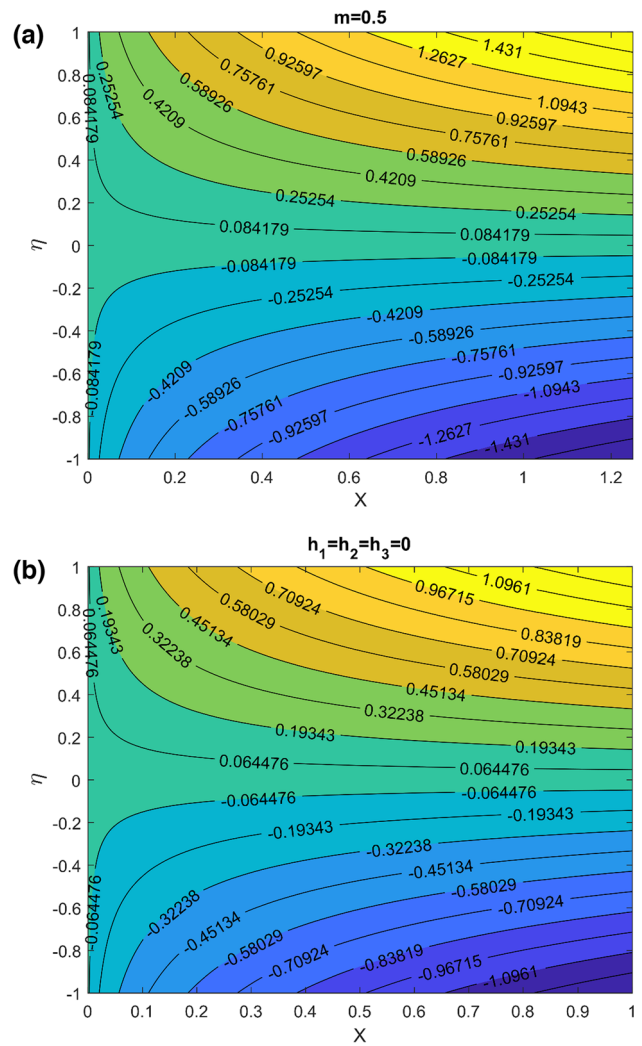
Fig. 20 Streamlines whenever $M = 5$

Fig. 21 Streamlines whenever $h_1 = h_2 = h_3 = 0$

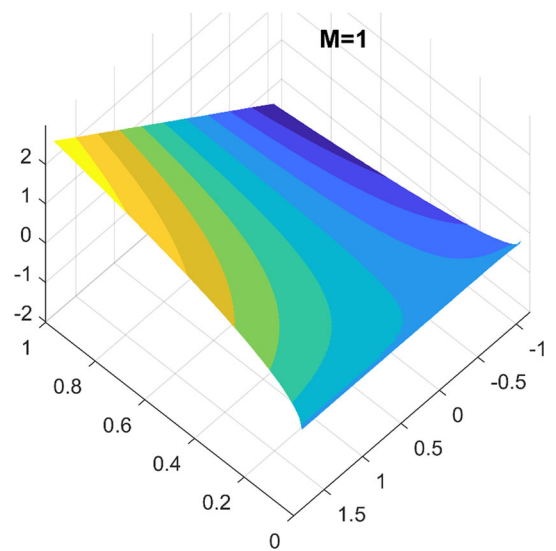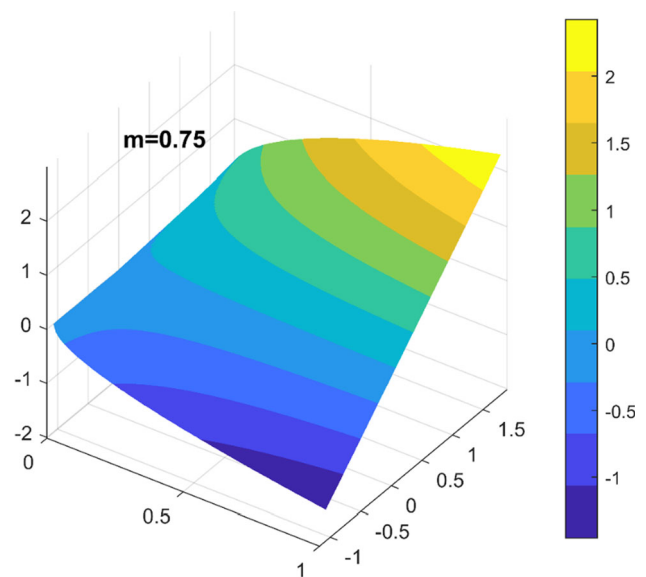**Fig. 22** Velocity boundary layer whenever $M = 5$

Fig. 23 Velocity boundary layer whenever **a** $m = 0.5$, **b** $h_1 = h_2 = h_3 = 0$

Fig. 24 Surface plot whenever $M = 1$

Fig. 25 Surface plot whenever
$m = 0.75$

5 Conclusion

Williamson fluid and Casson fluid are of particular importance in the fields of industrial and biomechanical engineering. Due to its importance, the main motivation of this study is to propose a numerical solution to analyze the heat and mass transfer generation of MHD Casson and Williamson fluids through slender surfaces in the presence of multi-slip conditions. This research can be used to automate manufacturing and design processes based on viscosity properties. The governing equations of the flow are transformed by fitting similar variables and solved using the implicit finite difference method. This study analyzes the flow, heat, and mass transfer characteristics of Williamson and Casson fluid across a slender horizontal surface with variable thickness. The coefficient of skin friction, heat, and mass transfer rate are examined. The observations of the characteristics are as follows:

- Williamson liquid is extremely simulated by the magnetic impact when associated with Casson liquid.
- The behavior of MHD, cross-diffusion, and multi-slip condition with slender sheets are incorporated in this physical model.
- The profile thickness of all the boundary layers of Williamson and Casson fluids is non-uniform, especially in the case of the velocity power index parameter.
- The impact of slip condition is high in the case of the Williamson motion in association with the Casson motion.
- In the nonexistence of the velocity slip parameter, temperature and concentration jump parameter thickness remain unchanged. It shows the similarity profile.

References

1. C. Béghein, F. Haghighat, F. Allard, Numerical study of double-diffusive natural convection in a square cavity. Int. J. Heat Mass Transf. **35**(4), 833–846 (1992)
2. X. Qiang, I. Siddique, K. Sadiq, N.A. Shah, Double diffusive MHD convective flows of a viscous fluid under the influence of the inclined magnetic field, source/sink, and chemical reaction. Alex. Eng. J. **59**, 4171–4181 (2020)
3. G. Sreedevi, R.R. Rao, D.R.V.P. Rao, A.J. Chamkha, Combined influence of radiation absorption and Hall current effects on MHD double-diffusive free convective flow past a stretching sheet. Ain Shams Eng. J. **7**, 383–397 (2016)
4. A. Sathiyamoorthi, S. Anbalagan, Mesoscopic analysis of heat line and mass line during double-diffusive MHD natural convection in an inclined cavity. Chin. J. Phys. **56**(5), 2155–2172 (2018)
5. G.H.R. Kefayati, Simulation of double-diffusive MHD (magnetohydrodynamic) natural convection and entropy generation in an open cavity filled with power-law fluids in the presence of Soret and Dufour effects (Part I: Study of fluid flow, heat, and mass transfer). Energy **107**, 889–916 (2016)
6. P. Mondal, T.R. Mohapatra, MHD double-diffusive mixed convection and entropy generation of nanofluid in a trapezoidal cavity. Int. J. Mech. Sci. **208**, 106665 (2021)
7. S.P.A. Devi, M. Prakash, Thermal radiation effects on hydromagnetic flow over a slendering stretching sheet. J. Brazilian Soc. Mech. Sci. Eng. **38**(2), 423–431 (2016)
8. S.P.A. Devi, M. Prakash, Temperature-dependent viscosity and thermal conductivity effects on hydromagnetic flow over a slendering stretching sheet. J. Nigerian Soc. Math. Biol. **34**, 318–330 (2015)
9. J.V.R. Reddy, V. Sugunamma, N. Sandeep, Thermophoresis and Brownian motion effects on unsteady MHD nanofluid flow over a slendering stretching surface with slip effects. Alex. Eng. J. **57**, 2465–2473 (2018)
10. S. Elattar, M.M. Helmi, M.A. Elkotb, M.A. El-Shorbagy, A. Abdulrahman, M. Bilal, A. Ali, Computational assessment of hybrid nanofluid flow with the influence of hall current and chemical reaction over a slender stretching surface. Alexandria Eng. J. **61**, 10319–10331 (2022)

11. K.V. Prasad, K. Vajravelu, H. Vaidya, R.A. Van Gorder, MHD flow and heat transfer in a nanofluid over a slender elastic sheet with variable thickness. Results Phys. **7**, 1462–1474 (2017)
12. L.L. Lee, Boundary layer over a thin needle. Phys. Fluids **10**(4), 822–828 (1967)
13. T. Fang, J. Zhang, Y. Zhong, Boundary layer flow over a stretching sheet with variable thickness. Appl. Math. Comput. **218**, 7241–7252 (2012)
14. M.T. Akolade, T.L. Oyekunle, H.O. Momoh, M.D.M. Awad, Thermophoretic movement, heat source, and sink influence on the Williamson fluid past a Riga surface with positive and negative Soret-Dufour mechanism. Heat Transfer **51**(5), 4228–4246 (2022)
15. M. Elayarani, M. Shanmugapriya, P. Senthil Kumar, Intensification of heat and mass transfer process in MHD Carreau nanofluid flow containing gyrotactic microorganisms. Chem. Eng. Process. Process Intensif **160**, 108299 (2021)
16. T. Hayat, R.S. Saif, R. Ellahi, T. Muhammad, A. Alsaedi, Simultaneous effects of melting heat and internal heat generation in stagnation point flow of Jeffrey fluid towards a nonlinear stretching surface with variable thickness. Int. J. Therm. Sci. **132**, 344–354 (2018)
17. N.S. Yousef, A.M. Megahed, N.I. Ghoneim, M. Elsafi, E. Fares, Chemical reaction impact on MHD dissipative Casson-Williamson nanofluid flow over a slippery stretching sheet through porous medium. Alex. Eng. J. **61**, 10161–10170 (2022)
18. A. Wakif, A novel numerical procedure for simulating steady MHD convective flows of radiative casson fluids over a horizontal stretching sheet with irregular geometry under the combined influence of temperature-dependent viscosity and thermal conductivity. Math. Prob. Eng. **2020**, 1675350 (2020)
19. M.T. Akolade, Y.O. Tijani, A comparative study of the three-dimensional flow of Casson-Williamson nanofluids past a Riga plate: Spectral quasi-linearization approach. Partial Diff. Equ. Appl. Math. **4**, 100108 (2021)
20. H.A. Ogunseye, S.O. Salawu, E.O. Fatunmbi, A numerical study of MHD heat and mass transfer of a reactive Casson-Williamson nanofluid past a vertical moving cylinder. Partial Diff. Equ. Appl. Math. **4**, 100148 (2021)
21. G. Kumaran, N. Sandeep, Thermophoresis and Brownian moment effects on the parabolic flow of MHD Casson and Williamson fluids with cross-diffusion. J. Mol. Liq. **233**, 262–269 (2017)
22. E. Seid, E. Haile, T. Walelign, Multiple slips Soret and Dufour effects in fluid flow near a vertical stretching sheet in the presence of magnetic nanoparticles. Int. J. Thermofluids **13**, 100136 (2022)
23. T. Thumma, O.A. Beg, A. Kadir, Numerical study of heat source/sink effects on dissipative magnetic nanofluid flow from a non-linear inclined stretching/shrinking sheet. J. Mol. Liq. **232**, 159–173 (2017)
24. T. Thumma, A. Wakif, I.L. Animasaun, Generalized differential quadrature analysis of three-dimensional MHD radiating dissipative Casson fluid conveying tiny particles. Heat Transf. Asian Res. **49**(5), 2595–2626 (2020)
25. M.M. Khader, A.M. Megahed, Numerical solution for boundary layer flow due to a nonlinearly stretching sheet with variable thickness and slip velocity. Eur. Phys. J. Plus **128**, 100 (2013)
26. M.J. Babu, N. Sandeep, MHD non-Newtonian fluid flow over a slendering stretching sheet in the presence of cross-diffusion effects. Alex. Eng. J. **55**(3), 2193–2201 (2016)
27. G. Aliy, N. Kishan, Optimal homotopy asymptotic solution for cross-diffusion effects on slip flow and heat transfer of electrical MHD Non-Newtonian fluid over a slendering stretching sheet. Int. J. Appl. Comput. Math. **5**, 80 (2019)
28. R.P. Sharma, K. Avinash, N. Sandeep, O.D. Makinde, Thermal radiation effect on Non-Newtonian fluid flow over a stretched sheet of Non-uniform thickness. Defect Diffus Forum **377**, 242–259 (2017)